2014-07-15

Weld residual stresses near the bimetallic interface in clad RPV steel: A comparison between deep-hole drilling and neutron diffraction data

James, MN

10.1016/j.nucengdes.2014.03.042
Nuclear Engineering and Design

Weld residual stresses near the bimetallic interface in clad RPV steel: A comparison between deep-hole drilling and neutron diffraction data

M N James [1, 3], M Newby [2], P Doubell [2], D G Hattingh [3], K Serasli [4] and D J Smith [4]

Abstract:
The inner surface of ferritic steel reactor pressure vessels (RPV) is clad with strip welded austenitic stainless steel primarily to increase the long-term corrosion resistance of the ferritic vessel. The strip welding process used in the cladding operation induces significant residual stresses in the clad layer and in the RPV steel substrate, arising both from the thermal cycle and from the very different thermal and mechanical properties of the austenitic clad layer and the ferritic RPV steel This work measures residual stresses using the deep hole drilling (DHD) and neutron diffraction (ND) techniques and compares residual stress data obtained by the two methods in a stainless clad coupon of A533B Class 2 steel. The results give confidence that both techniques are capable of assessing the trends in residual stresses, and their magnitudes. Significant differences are that the ND data shows greater values of the tensile stress peaks (~100 MPa) than the DHD data but has a higher systematic error associated with it. The stress peaks are sharper with the ND technique and also differ in spatial position by around 1 mm compared with the DHD technique.

Keywords: RPV cladding; residual stress; neutron diffraction; deep-hole drilling

Introduction

The inner surface of ferritic steel reactor pressure vessels (RPV) is clad with strip welded austenitic stainless steel primarily to increase the long-term corrosion resistance of the ferritic vessel. The potential problem with corrosion in the presence of boric acid in low alloy RPV steels is well-illustrated by the corrosion found in the RPV head at the Davis-Besse nuclear power station [1]. The RPV head was manufactured from A533B Grade 1 steel that was clad with Type 308 stainless steel. Xu et al [1] report that some 4,261 cm^3 of material had been removed from the inner surface of the RPV head by boric acid corrosion. An additional benefit, as noted by Sattari-far and Andersson [2], arises because the austenitic layer has a lower value of thermal conductivity than the ferritic substrate, and hence the clad layer can also act as a thermal barrier in the event of a thermal shock. This reduces the thermally induced stresses at the inner surface of an RPV subjected to such a thermal shock event.

The strip welding process used in the cladding operation induces significant residual stresses in the clad layer and in the RPV steel casing, arising both from the thermal cycle and from the very different thermal and mechanical properties of the austenitic clad layer

[1] School of Marine Science & Engineering, University of Plymouth, Drake Circus, Plymouth, UK
[2] Eskom Holdings SOC Ltd Lower Germiston Road, Rosherville Johannesburg, South Africa
[3] Department of Mechanical Engineering, Nelson Mandela Metropolitan University, Port Elizabeth, South Africa
[4] Department of Mechanical Engineering, University of Bristol, Queen's Building, University Walk, Bristol, UK.

and the ferritic RPV steel [3]. In structural integrity terms it is important to characterise the magnitude and distribution of these residual stresses as they can impact upon the possibility of brittle fracture and stress corrosion cracking. In this respect, current codes for assessing the structural integrity of an RPV often do not adequately consider residual stresses [3, 4]. For instance, Katsuyama et al [4] state that the Japanese code stipulates a rule based on fracture mechanics to assess an RPV against the possibility of brittle fracture under pressurised shock events, but also note that the code contains no provision for residual stresses. With this in mind, there have been a number of studies that have sought to assess weld-induced residual stresses arising from the cladding process, particularly in the context of the possible growth and influence on fracture of defects near the cladding interface. Reference 5 describes the density and distribution of typical fabrication defects found at weld repairs to reactor pressure vessels, many of which occur either in the cladding or at the surface of the RPV steel and which will therefore be influenced by cladding-induced residual stresses. In this respect, Hohe et al [3] have reported work on the effect of cladding and the related residual stress field on the fracture behaviour of 74 mm thick plates of A508 grade steel, strip welded with a double layer of austenitic cladding 8 mm thick in total. They found that a sub-cladding crack in the ferritic alloy was more critical in terms of brittle fracture, than a through-cladding crack which exhibited interim crack initiation and arrest prior to final fracture at a higher load than that observed for the sub-cladding crack.

Katsayama et al [4] presented residual stress data from a finite element (FE) model of part of a 3-loop RPV made of ASTM A533B Grade 1 steel clad with Type 309L stainless steel. They considered both submerged arc welding (SAW) and electroslag welding (ESW). Their model involved a thermal-elastic-plastic-creep analysis that incorporated the phase transformation which occurs in the high temperature heat-affected zone (HAZ). They also compared their FE results with experimental data obtained by deep-hole drilling (DHD). In the as-welded ESW case they obtained tensile longitudinal residual stresses in the cladding, with compressive stress peaks occurring just below the cladding and then tensile stresses in the bulk of the ferritic steel. Peak values of longitudinal tensile stress of around 275 MPa occurred in the RPV steel at the intersection of the strip welding runs, with peak longitudinal compressive stresses located more towards the centre of the weld runs. Compressive peak residual stresses in the ferritic steel with values of around 150 MPa were observed.

A significant issue in measuring residual stresses at joints between dissimilar metals is the large variability often seen in the results obtained by different methods. For instance, Ogawa et al [6] compared axial and hoop residual stress data obtained from FE modelling and DHD of stainless steel cladding on a low alloy steel nozzle forging. Although the general shape of the FE and DHD residual stress distributions were similar, the peak values in the axial direction were some 200 MPa higher with the FE model than those measured with the DHD method. Deng et al have also presented a 2D FE model of a clad joint between thick walled low alloy and stainless steel pipe [7]. They considered a wide range of possible joint options, and in certain cases found yield strength magnitude values of tensile axial residual stress in the cladding, even after post-weld heat treatment (PWHT). Their conclusions suggested that the final residual stresses in the outer surface of the pipe near the weld zone were not greatly influenced by the welding or PWHT processes, but that significant variability was found in the residual stresses at the inner surface. They stated that the results from their FE model agreed reasonably well with their limited surface strain gauge measurements made using a wire cutting technique.

In application to thick section components, the DHD and neutron diffraction techniques for measuring residual stress appear to be the most promising. The deep-hole drilling technique is described in reference 8 and can provide 2D residual stresses in the transverse and longitudinal directions across the complete RPV wall thickness. The use of neutron diffraction strain scanning for measuring residual stress is detailed in reference 9, and the technique can provide 3D information over depths of steel of up to 60-80 mm [10]. In neutron strain scanning the residual stress data is obtained from a cubic volume typically ~1 mm^3 and samples with a mass of up to 900 kgf can be accommodated by the latest generation of strain scanning instruments, while the measurement gauge volume can be moved around in the specimen with a precision of some 10 µm. The DHD technique can be used on reactor pressure vessels in-situ at a power station and is therefore very useful, while the neutron strain scanning technique requires an RPV coupon to be brought to the neutron diffraction beamline.

However, the ability to accurately measure residual stress across the cladding-ferritic steel interface by measuring changes in diameter of the drilled hole in the DHD method [8, 11] requires validation. For example the change in elastic modulus and mechanical properties at the interface complicate the determination of residual stresses in a stainless clad ferritic steel plate. The purpose of this work was therefore to compare the residual stress data obtained via neutron diffraction strain scanning and by the DHD technique in a stainless clad coupon of A533B Class 2 steel.

The sample used in this work was an original stamped and numbered reactor pressure vessel coupon obtained by Eskom when they commissioned their Framatome 900 MWe nuclear reactor pressure vessels installed at the Koeberg power station in South Africa. This coupon had the form of an 80 mm thick slice of A533B Class 2 steel, some 580 mm long, taken through the reactor wall (≈240 mm thick). This coupon is shown in Figure 1 and it should be noted that the cladding in this work has been applied to the steel coupon on a face at 90° to the surface that would be clad in an operating reactor. This was done because the thickness of the coupon slice (80 mm) was too small to allow development of the full residual stress magnitudes that would be associated with large-scale stainless strip-weld cladding. For a clad region measuring some 580 x 240 mm, however, the residual stress field obtained after welding is likely to be representative of the as-welded state in an operating RPV.

In particular, it was desired to accurately measure the residual stresses across the critical cladding-RPV steel interface region using the neutron strain scanning technique and compare the data with that obtained from the DHD method.

Specimen Preparation

The stainless steel cladding was laid down using submerged arc welding (SAW) with the same filler metal alloys and a similar procedure to that used in the Koeberg reactor pressure vessels. Weld metal properties in the initial cladding layers are strongly influenced by dilution of the filler metal from the higher carbon and lower chromium and nickel content of the parent plate. In order to achieve low carbon content in the overlay, initial buttering layers are used to minimise carbon dilution in subsequent layers. Initial weld buttering therefore

used Soudotape 309L (ASME II SFA 5.9 Grade EQ309L) filler metal to deposit a cladding layer some 4.5 mm thick. This was followed by a deposit of Soudotape 308L (ASME II SFA 5.9 Grade EQ308L) filler metal to provide another layer of cladding also around 4.5 mm thick. The final depth of stainless cladding was therefore some 9 mm. The 309L is used as the buttering layer because of the higher Cr and Ni content, compared with 308L, which is better able to counter dilution effects of the low alloy ferritic steel (see Table 1).

Run-on and run-off tabs were tack welded to all four sides of the plate prior to commencing the cladding process. Surface preparation involved machining and degreasing, with interpass brushing. Table 1 gives chemical composition for the A553B Class 2 steel, while Table 2 gives typical mechanical property data and Table 3 details the submerged arc welding conditions. The elastic modulus for the ferritic steel was taken as 212.7 GPa, and for the austenitic steel as 195 GPa with Poisson's ratio taken as 0.28. The welding flux was Record INT 101 conforming to EN760 Grade SA-AB 2Cr and DC electrode-positive welding was used. According to Sattari-far and Andersson [2] the positive polarity on the strip electrode increases penetration and reduces the risk of welding defects in the weld run overlap zones through providing a thinner weld bead and consequently, more shallow bead edges. Figure 2 shows the coupon with run-on and run-off tabs attached, in position for strip welding after laying down two weld runs.

After completing the cladding process, the plate was subsequently reduced in size and thickness to allow neutron diffraction measurements to be made in the 5 days of neutron diffraction beamtime time allocated to ILL experiment 1-02-44 on the SALSA instrument. A schematic showing the position of these two cuts is given in Figure 3, with the first cut reducing the overall size of the residual stress specimen to 250 x 240 x 80 mm, and the second cut reducing the thickness of the ferritic steel under the cladding layer to approximately 40 mm which was then further reduced by grinding to 30 mm. With an average cladding thickness of approximately 9 mm, the overall final thickness of the block was approximately 39 mm which is believed to be sufficient to retain a significant as-welded residual stress magnitude across the bimetallic interface region. Although cutting the plate will reduce the overall magnitude of the residual stress field, the prime intention in this paper was to compare the residual stress measurements using neutron diffraction strain scanning with those made via DHD. It would also be expected that the general shape and trends observed in the residual stress profile across the weld zones would be retained. However, as noted below, the strain relaxation was measured using strain rosettes and this data was used to provide an estimate of the relaxation in an assumed equibiaxial through-thickness bending stress.

In order to obtain an estimate of the relaxation in residual stress arising from this reduction in size and thickness, before any machining was undertaken the weld-clad coupon was strain gauged on the top and bottom surfaces with four strain rosettes (Figure 1 shows the two rosettes on the bottom surface). The change in strain readings was measured relative to the initial state of the clad coupon after making each of the two cuts. Table 4 gives the measured changes in strain and the resulting calculated change in values of the two principal stresses at the plate surface resulting from each cut, for the plate section used for the neutron strain scanning measurements. As expected, the first cut causes only a minor change in principal stress level at the centre of each of the two halves of the coupon,

although the direction of the most positive principal stress is rotated relatively by some 73° on the two opposite sides of the plate.

A more substantial change in principal stresses occurs after the second cut which reduced the plate thickness from 80 mm to 40 mm. Table 4 indicates that both principal residual stresses at the plate surfaces experience a substantial compressive change as a result of this cut. This implies that the value of surface residual stresses measured during neutron diffraction strain scanning would be less tensile than would have been the case if the plate had not been thinned.

Strain-free Reference (d_0) Specimens

In making neutron diffraction strain measurements for welded specimens with graded microstructures, determination of the strain-free lattice spacing d_0 is important. The Bragg equation relates the position of a diffraction peak to the crystal lattice spacing and is given by:

$$2d_{\{h\ k\ l\}} \sin(\theta) = \lambda \tag{1}$$

where λ is the wavelength of the neutron radiation, θ is half the scattering angle and $d_{\{h\ k\ l\}}$ is the lattice spacing for the set of planes used to diffract the neutron beam. Strain is simply obtained from the equation:

$$\varepsilon = \frac{d_{\{h\ k\ l\}} - d_{0\{h\ k\ l\}}}{d_{0\{h\ k\ l\}}} \tag{2}$$

In practice the wavelength remains constant during a neutron diffraction experiment and equation 2 may be reduced to:

$$\varepsilon = \frac{\sin(\theta_{d_{0\{h\ k\ l\}}})}{sin(\theta_{\{h\ k\ l\}})} - 1 \tag{3}$$

where $d_{0\{h\ k\ l\}}$ is the strain-free lattice spacing for the *{h k l}* planes.

In the present work the strain-free lattice spacing in the interface region across the weld was determined using 3 mm cubes of material obtained in the following manner. Figure 4 shows the clad surface of the coupon after removing the side tabs and the quadrilateral-shaped piece outlined in yellow was cut via electro-discharge machining (EDM) and used to obtain a toothcomb specimen from which the cubes were cut. Figure 5 shows diagrams illustrating the process of obtaining strain-free reference cubes. Figure 5a shows the central 3 mm thick slice which was excised from the quadrilateral piece via EDM, and then polished and etched to identify the fusion boundary. The toothcomb shape shown in Figure 5b was then cut by EDM and 3 mm cubes were cut off the ends of the teeth to provide the required strain-free reference specimens. Four groups of three d_0 blocks were used in the neutron diffraction measurements, respectively in the *x*, *y*, and *z* coordinate directions (where the *x*-direction is longitudinally along the weld run, *y* is the direction transverse to the weld run and

z is the through-thickness or short-transverse direction in the plate), representing the parent metal, the heat affected zone (HAZ), the fusion line and the 309L weld metal.

Neutron Diffraction (ND) Strain Scanning

This was performed at the ILL in Grenoble, France on the SALSA instrument, which is a world-leading neutron instrument for the assessment of residual stress in large scale engineering components. One of the principal challenges during strain scanning experiments relates to moving the specimen gauge volume about relative to the neutron beam. SALSA uses a unique hexapod stage design with six independently driven hydraulic legs which can move a specimen with a mass of up to 900 kgf with a precision of the order of 10 µm. During the experiment (1-02-44) the wavelength of the neutron radiation was 1.648 Å and the reactor power was 52.4 MW. Initially it was hoped to make 3D residual stress measurements at two positions in the clad plate, with position 1 being in the centre of the plate and in the middle of a weld run, while position 2 was located 45 mm in the *x*-direction and 30 mm in the *y*-direction from position 1, at the intersection of two weld runs. These positions were chosen because of the differences noted by Katsayama et al [4] in the interfacial residual stress values at these two positions. However it proved difficult to obtain good diffraction peak data at position 1, presumably due to weld texture effects, so attention was focused on the weld run intersection at position 2.

Strain measurements were made in all three coordinate directions at a matrix of points with the back face of the clad plate taken as the *z*-direction zero datum. Measurements were made at 5 mm steps from this datum between z = 5 mm to z = 25 mm, and then at 1 mm steps from z = 25 mm to z = 36 mm. The gauge volume of 0.6x0.6x2.0 mm was defined by collimators of 0.6 mm and a 2 mm slit, with the 0.6 mm dimension being maintained in the z-direction for all the scans to provide sufficient spatial resolution across The small gauge volume was required to give sufficient spatial resolution across the cladding-ferritic steel interface. This leads to higher errors than are usually obtained with a larger gauge volume, as indicated by the error bars on Figures 6 and 7. However, error was mainly affected by path length, not gauge volume. Thus in Figure 7 the error in the Z-direction stress at 10 mm depth is approximately 66% higher than at 5 mm depth, purely due to path length as both points are in the ferritic parent material. At measurement depths into the plate < 15 mm (a path length of approximately 21 mm), a good peak could be obtained either 6,000 neutron counts or one hour of measurement time. However, at a depth of 20 mm (a path length of approximately 55 mm) this counting time was insufficient and the neutron count was increased to 12,000 and the time out to two hours. These parameters were also used for the transmission scans. This resulted in acceptable peak statistics.

The (2 1 1) diffraction planes were used for measurements in the ferritic alloy while the (3 1 1) planes were used in the austenitic stainless steel clad layers. These planes are useful as they provide an ‘averaged’ response of the crystal lattice to applied stresses. To allow for mechanical property change and dilution effects near the fusion boundary, diffraction measurements across the interface region were made using both sets of lattice planes for points between z = 28-30 mm.

The results of the residual stress measurements are given in Figures 6 and 7 and they will be discussed in terms of the influence of the various weld layers later in the paper. Typical error bars are also shown in these figures, with strain values lying in the range ±110-150

microstrain and stress values lying in the range ±30-70 MPa. Note that distances are given relative to the rear (unclad) surface of the plate, and hence 40 mm represents the surface of the weld overlay cladding. The raw data was processed using the ILL beam line software LAMP (large array manipulation program) using a pseudo-Voigt curve fitting algorithm for the peak position. The strain measurement errors were calculated on a point by point basis from the peak position uncertainty generated by the LAMP software. A disadvantage of the small gauge volume was the increase in strain measurement errors as the beam path length increased, illustrated in Figure 6 by the z-direction scan where the path length varies from the outside to the centre of the sample.

Deep-Hole Drilling (DHD)

After the non-destructive neutron diffraction residual stress measurements were concluded, the plate was sent to the University of Bristol so that the residual stresses could be assessed using the semi-destructive DHD measurement technique. The DHD technique measures the distortion of a small diameter reference hole drilled through the component. The hole diameter is accurately measured at a number of angles and a number of points through the thickness. A cylindrical core which contains the reference hole is then trepanned out of the component and changes in diameter of the hole and in column length are measured. Trepanning the cylindrical core releases residual stresses and changes in the hole diameter and column length are converted to strains, and hence to stresses. It is assumed that the axis of the reference hole is a principal stress direction and that stress relaxation at the hole edge is elastic. Leggatt et al [12] give full details of the process.

Residual stress measurement using DHD was performed at the same position as the 3D neutron diffraction measurements, i.e. the weld run intersection at position 2 and the drilling process started from the clad surface (see Figure 8). The DHD technique utilised a 1.5 mm diameter reference gun drilled hole and a 5 mm diameter trepanned core, which was removed by electro-discharge machining (EDM) using a copper electrode. In the standard DHD technique hole diameter measurements are made every 0.5 mm of drilled depth, and there was an interest in this work in comparing the results with those obtained from an incremental deep-hole drilling method (iDHD). It is now known that plasticity can occur during the application of the standard DHD method [11]. To overcome this problem the iDHD method involves making incremental measurements. For the clad weld specimen this involved making measurements at 13 steps through the plate thickness, initially in approximately 2 mm steps to 10 mm and then in 3 mm steps to 36 mm. Initial increments over the first 10 mm were closer to each other because this was deemed to be the critical region in residual stress terms. The 2D residual stress data obtained with the DHD technique are shown in Figure 9 and the results obtained by the two DHD methods are reasonably similar and do not reveal evidence of plasticity influencing the data during measurement. Typical stress errors in this data are ±25 MPa, which is significantly smaller than those observed in the neutron diffraction stress data. However, this lower value of systematic error in DHD measurements may be offset by higher potential errors in the model used to transform pressure changes into displacements and hence into stresses that arise from the change in elastic modulus and mechanical properties at the interface.

Figure 10 shows the effect of reducing the thickness of the plate from 80 mm to 30 mm and this data is based on the change in residual strain recorded using strain rosettes attached to

the plate surfaces prior to cutting. This graph is based on the presence of an approximately equibiaxial through-thickness bending stress field, which is relaxed during cutting. This leads to a reduction in the residual stress on the clad surface and an equivalent increase in the residual stress on the cut surface.

Metallurgical and Residual Stress Details

Once all the residual stress measurements were completed a rectangular section (with one corner coinciding with the position of the DHD core) was removed from the plate by electrodischarge machining (EDM). Slices were then cut from this by EDM to provide two slices of plate approximately 10 mm thick that were representative of the various metallurgical layers in both the transverse direction to the weld and along the weld run. Figure 11 shows the relative position of these slices in the original plate. The slices were etched using Marble's reagent, a mixture of copper sulphate, hydrochloric acid and water. This made it straightforward to measure the width of the heat affected zone (HAZ) and the two layers of stainless steel weld metal. As the diameter of hole in the plate left by the DHD coring process is some 6 mm the precise thickness at the original neutron diffraction measurement point has to be estimated from measurements made at the edge of the DHD hole. Figure 12 shows macroetched sections of the weld profile parallel with the weld run direction (Figure 12a) and transverse to the weld run (Figure 12b). The depths of the cladding layers of 308 and 309 stainless steel and the HAZ could be measured using standard image analysis techniques, and the various layers and metallurgical boundaries are shown in Figure 12a. The various metallurgical layers are defined in Figures 11 and 12 as parent plate (PP), heat affected zone (HAZ), grade 308L weld metal (308) and grade 309L weld metal (309).

The neutron diffraction measurements were made taking the back face of the plate as a datum line, while the DHD measurements were made from the front clad surface for obvious reasons of accuracy of hole location. It was therefore necessary to determine the distance of the clad surface from the back face at the original ND measurement point. This was done by measuring the plate thickness either side of the DHD hole and averaging the two measurements. This allowed the DHD residual stress profile to be accurately positioned relative to the ND profile and for peaks in the data to be correlated with the various metallurgical interfaces.

At the original ND measurement position, the parent plate HAZ is hence estimated to begin approximately 21.3 mm from the back face of the plate, the weld fusion boundary to be 29.1 mm from this datum, the boundary between the 309 and 308 stainless steel layers to be 32.8 mm from the back face and surface of the cladding layer to be 38 mm from the datum. The macroetched images indicate that the actual thickness of the cladding layer varies between about 8-10 mm depending on position in the cladding weld runs, being thicker towards the centre of the weld strip (which is 60 mm wide – Table 3).

Lines representing the approximate position of these various metallurgical interfaces are shown in Figure 7 which presents the ND residual stress data measured at the intersection point of two weld runs (*x*-direction being longitudinal and *y*-direction transverse with respect to the weld run). It is clear that tensile peaks in the residual stress profiles correlate fairly closely with the HAZ, fusion and 309/308 boundaries and that peak compressive stresses

occur several millimetres either side of the fusion boundaries (HAZ/309 and 309/308). It is also clear the shape of the residual stress profile in the three coordinate directions over this section of the plate is very similar with prime differences being only the magnitude of the tensile and compressive peaks. These trends agree with those reported by Katsayama et al [4], who reported tensile longitudinal residual stresses in the stainless cladding, with compressive stress peaks occurring just below the cladding and then tensile stresses in the bulk of the ferritic steel. They also observed peak tensile longitudinal stress values at the intersection of two weld runs as 275 MPa which corresponds well with the value measured in this work using ND (282 MPa). Katsayama et al [4] also observe that peak longitudinal compressive stresses were located more towards the centre of a weld run. As noted earlier in this paper, it had been hoped to measure the 3D residual stresses at two points in the plate, with position 1 being at the centre of a weld run. However, difficulties were experienced in obtaining diffraction peaks at this position and, in the experiment time available, only data for position 2 (weld run intersection) was obtained.

It has to be remembered, in considering the data shown in Figure 7, that the apparent lack of a force balance in the residual stress field arises because of the partial nature of the residual stresses shown which cover less than 10% of the plate dimensions.

Several other authors have previously reported residual stress data obtained from similar plates of stainless clad ferritic steel. For instance, Dupas and Moinereau [13] considered plates of A508 steel clad with a 3.5 mm thick buttering layer of 309L and then a second 4 mm thick layer of 308L stainless steel. They used a number of specimens, intended to simulate a reactor pressure vessel, which had different dimensions (typically 510 mm long, 560 mm wide and 85 mm thick), and a variable number of weld strips and layers. Residual stresses were measured by several destructive techniques, and were generally found to follow a pattern of high tensile in the weld metal, compressive in the HAZ and high tensile at the interface between the HAZ and the substrate metal. The authors acknowledged that there is a substantial variability between residual stress data obtained using the two different techniques employed in their work.

These same residual stress trends in moving from the weld metal through the HAZ to the substrate metal, can also be observed in the data shown in Figures 7 and 9, although the ND results appear to show a better resolution of these trends between the various alloy layers than the DHD data.

The data reported by Dupas and Moinereau [13] also lend support to the point made earlier in the paper that reducing the thickness of the block would be expected to reduce the magnitude of peaks in the data but should not change the general shape of the residual stress profile.

A recent PhD study by Ohms [14] performed measurements of residual stress on a rectangular block of ferritic steel clad with 10 mm of austenitic stainless steel deposited as three layers each around 3.5 mm thick. The ferritic steel block was 450 mm long, 250 mm wide and 136 mm thick. Residual stresses were measured using ND, DHD and the ring core method. The ferritic block was thinned after cladding to 25 mm and a gauge volume of 2x2x20 mm3 was used in the ND work. Measurements of the strain-free lattice spacing were made on 3 mm thick slices cut from several positions on the block. Ohms used the (1

1 0) lattice planes for measurements in the ferritic steel and (2 0 0) planes for the austenitic steel.

The residual stress data measured by Ohms using ND show the same trends in the three layers of austenitic steel cladding as those observed in the present work, i.e. localised tensile peaks at the interfaces and compressive peaks towards the centre of the layers, although the average value of residual stress was higher in their measurements, lying between 300 MPa and 400 MPa. Ohms did not average data across the interface between the ferritic steel and the cladding, and so did not present data in this important region.

The DHD residual stress data reported by Ohms support the observations made in this paper that the DHD technique does not detect the peaks and troughs observed in the cladding layers but does reproduce the overall trends seen in the ND results. It is also the case that his DHD data show the similar trends relative to the ND results as the data shown in Figure 13; namely that the two techniques give similar results in the austenitic weld metal and are consistently different in the ferritic steel. We believe that these differences may reflect the different volumes over which the strains are averaged in the various techniques. For example, the DHD technique used in the present work utilised a 1.5 mm diameter reference hole and a 5 mm diameter trepanned core, whilst that used by Ohms involved a 3.18 mm reference hole and a 10 mm diameter core.

The observation that the x-direction (longitudinal) residual stress in Figures 7 and 9 may be generally slightly higher than the y-direction (transverse) residual stress can be ascribed to the relative length of a weld strip in those two directions, but the size and overlap of the error bars on the data mean that any absolute comparison is unreliable.

Comparison between Residual Stress Techniques

Figure 13 shows a comparison between the neutron diffraction and DHD measurements of residual stress through the thickness of this austenitic clad RPV plate. The general trends in the residual stress distribution are similar, but there are significant differences of detail. In particular, the neutron diffraction strain scanning indicates a generally higher level of tensile residual stress across most of the ferritic A533B steel in both the longitudinal (X) direction and transverse (Y) directions than is shown by the DHD technique. In addition, the ND technique shows sharper compressive and tensile peaks, which could be a result of the limited number of spatial data points used in the ND work. There is close agreement between the two techniques, however, on the magnitude of the minimum value of the longitudinal stress which occurs in the ferritic steel some 3 mm before the fusion boundary, although there is a spatial disagreement of about 1 mm in its position between the two techniques. The DHD technique does not reveal the transient tensile stress at the fusion boundary, which is shown by the neutron diffraction strain scanning technique, nor does it appear to replicate the compressive peak observed in the ND data in the austenitic weld metal approximately 2 mm past the fusion boundary. The DHD results indicate that these sharp variations in stress are not measured by the technique. This is not surprising since the core size for the DHD method was about 5mm, and as can be seen in Figure 13, the variations occur over similar distances. At the 308L-309L fusion boundary a slight dip in the DHD data is observed, but not the sharp minimum seen in the ND strain scanning data. In summary it appears that neutron diffraction strain scanning gives more sharply defined

peaks in the residual stress profile and that it gives residual stress values generally around 100 MPa higher than the DHD data.

Conclusions

This work has measured the residual stresses associated with the stainless steel cladding on a ferritic steel RPV test coupon. Data has been acquired using two different techniques, neutron diffraction (ND) at the ILL site in Grenoble, France, using the SALSA instrument and deep-hole drilling (DHD) performed at the University of Bristol. The ND technique gives 3D data while the DHD technique can provide 2D data. Key conclusions are as follows:

1. The trends in the data are generally similar for the two techniques with an alternating sequence of negative and tensile peaks in moving across the various metallurgical boundaries in the weld region, i.e. parent plate to HAZ, HAZ to 309 stainless steel buttering layer, and 309 to 308 stainless steel.
2. Tensile peaks occur just before or at a metallurgical boundary while negative peaks occur more centrally in the various alloy layers.
3. The largest magnitude tensile transverse stress peak of some 255 MPa occurs near the parent plate (PP) to heat affected zone (HAZ) fusion boundary in the ferritic A533B steel, while the greatest magnitude compressive transverse stress of -120 MPa occurs in the 309 stainless steel buttering layer.
4. The ND data shows greater values of the tensile stress peaks (~100 MPa) than the DHD data but has a higher systematic error associated with it. The stress peaks are sharper with the ND technique and also differ in spatial position by around 1 mm compared with the DHD technique. A small compressive peak in the top cladding layer of 308 grade stainless steel has not been detected by the DHD technique.
5. These trends observed in the residual stress data agree with those reported by Katsayama et al [4] from their finite element analysis, who reported tensile longitudinal residual stresses in the stainless cladding, with compressive stress peaks occurring just below the cladding and then tensile stresses in the bulk of the ferritic steel.
6. The peak tensile longitudinal stress value of 282 MPa recorded using ND in the present work, at the intersection of two weld runs, corresponds well with the value found by Katsayama et al [4] (275 MPa) at a similar position using their numerical model of stainless clad ferritic steel.

The results give confidence that both techniques are capable of assessing the trends in residual stresses, and their magnitudes, in thick-walled reactor pressure vessels steels, with the choice of technique largely depending on the particular circumstances of each sample, i.e. either in-situ on an RPV or using a test coupon.

Acknowledgments

This work was performed at the ILL, Grenoble, under experiment 1-02-44 and the award of 5 days of beamtime on the SALSA instrument, along with the assistance of the beamline scientist Dr T Pirling, is gratefully acknowledged. The support of Eskom, South Africa

through the supply of the RPV steel coupon and performing the weld cladding is also gratefully acknowledged.

References

1. H Xu, S Fyfitch and J W Hyres (2005), *Boric acid corrosion laboratory investigation of the Davis-Besse reactor pressure vessel head*, Proceedings of the 12th International Conference on Environmental Degradation of Materials in Nuclear Power System – Water Reactors, Edited by T R Allen, P J King and L Nelson, The Minerals, Metals and Materials Society, TMS 2005.
2. I Sattari-far and M Andersson (2006), *Cladding effects on structural integrity of nuclear components*, SKI Report 2006:23, June 2006, Swedish Nuclear Power Inspectorate.
3. J Hohe, M Brand and D Siegele (2010), *Behaviour of sub-clad and through-clad cracks under consideration of the residual stress field*, Engineering Fracture Mechanics, Vol. 77, pp.217-228.
4. J Katsuyama, H Nishikawa, M Udagawa, M Nakamura and K Onizawa (2010), *Assessments of residual stress due to weld-overlay cladding and structural integrity of reactor pressure vessel*, Paper PVP2010-25541, Proceedings of the ASME 2010 Pressure Vessels & Piping Division / K-PVP Conference, July 18-22, 2010, Bellevue, Washington, USA.
5. G J Schuster, F A Simonen and S R Doctor (2008), *Fabrication flaw density and distribution in repairs to reactor pressure vessel and piping welds*, United States Nuclear Regulatory Commission, Report NUREG/CR-6945, PNNL-16726, April 2008.
6. N Ogawa, I Muroya, Y Iwamoto, T Ohta, M Ochi, K Hojo and K Ogawa (2012), *Studies of residual stress measurement and analysis techniques for a PWR dissimilar weld joint*, International Journal of Pressure Vessels and Piping, Vol. 90-91, pp.84-90.
7. D Deng, K Ogawa, S Kiyoshima, N Yanagida and K Saito (2009), *Prediction of residual stresses in a dissimilar metal welded pipe with considering cladding, buttering and post weld heat treatment*, Computational Materials Science, Vol. 47, pp.398-408.
8. D J Smith, P J Bouchard and D George (2000), *Measurement and prediction of residual stresses in thick-section steel welds*, Journal of Strain Analysis for Engineering Design, Vol. 35 No.4, pp. 287–305.
9. *Polycrystalline materials – determination of residual stresses by neutron diffraction*, ISO-TTA 3:2001, International Organisation for Standardisation, Geneva.
10. V Em, W Woo, B-S Seong, P Mikula, J Joo, M-H Kang and K H Lee (2012), *Residual stress determination in thick welded steel plates*, Journal of Physics, Conference Series Vol. 340, 012025, pp.1-6,
11. A H Mahmoudi, C E Truman, D J Smith, M J Pavier (2011), *The effect of plasticity on the ability of the deep-hole drilling technique to measure axisymmetric residual stress*, International Journal of Mechanical Sciences, Vol. 53, pp.978-988.
12. R H Leggatt, D J Smith, D S Smith and F Faure (1996), *Development and experimental validation of the deep hole method for residual stress measurement*, Journal of Strain Analysis, Vol. 31, pp.177-186.
13. P Dupas and D Moinereau (1996), *Evaluation of cladding residual stresses in clad blocks by measurements and numerical simulations*, Journal de Physique IV,

Colloque C1, supplement au Journal de Physique III, Vol. 6 January 1996, C1-187 – C1-196.

14. C Ohms (2013), *Residual stresses in thick bi-metallic fusion welds: a neutron diffraction study*, PhD thesis, Technical University of Delft.

Table 1 Typical chemical composition of alloys (wt%)

	C	Mn	Si	Cr	Ni	Mo	N	S	P	Fe
A533B	0.25	1.15-1.50	0.15-0.40	-	0.40-0.70	0.45-0.60	-	0.025	0.025	Bal.
309L	0.012	1.8	0.4	23.7	13.3	0.1	0.048			Bal.
308L	0.013	1.7	0.4	20.3	10.4	0.1	0.040			Bal.

Table 2 Typical mechanical properties

	Tensile Strength MPa	Yield Strength MPa	Elongation %
A533B Class 2	620-795	485	16
309L	585	415	37
308L	610	410	38

Table 3 Submerged arc welding conditions

	Strip Size (mm)	Preheat (°C)	Interpass Temperature (°C)	Welding Current	Strip Speed (m/min)	Travel Speed (mm/min)
Soudotape 309L	60 x 0.5	150	Min 200 Max 350	1320 A 27-29 V	2	230
Soudotape 308L	60 x 0.5	150	Min 200 Max 350	1350 A 27-29 V	2	280

Table 4 Change in strain at the coupon surfaces and equivalent stress change resulting from the two cuts

Condition	Gauge	Strain A (μm/m)	Strain B (μm/m)	Strain C (μm/m)	σ_1 (MPa)	σ_2 (MPa)	Θ_{σ_1} (°)
Test sample After 1st cut (Figure 3)	1	-26	-61	18	8.2	-10.4	124.4
Test Sample After 1st cut (Figure 3)	2	-24	-106	33	20.3	-17.6	127.8
Test Sample After 2nd cut (Figure 3)	1	-1525	-1567	-1261	-343.9	-410.6	116.4
Test sample After 2nd cut (Figure 3)	2	-1330	-988	-687	-244.4	-351.6	88.2

Note: The direction of σ_1 is anticlockwise relative to the longitudinal direction of the weld.

Figure 1 View of the A533B Class 2 steel coupon from the side opposite the cladding. The image shows the curved shape of the original RPV wall. It should be noted that in actual reactor use the cladding would be applied to the inner curved face.

Figure 2 View of the coupon after laying down two weld runs. The four edging tabs can be clearly seen in the image.

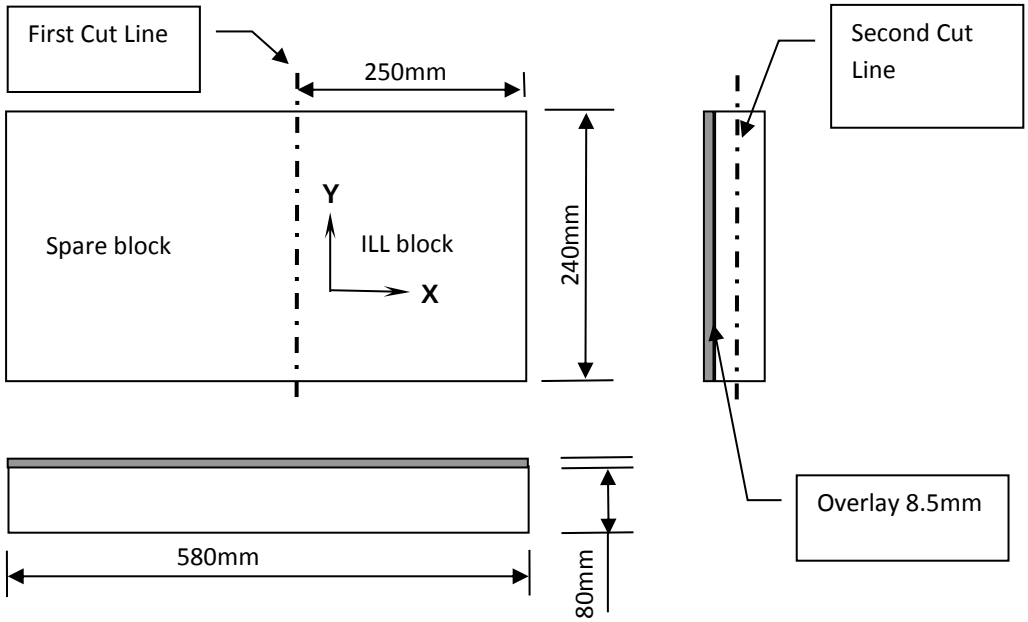

Figure 3 Schematic showing the two cuts made to the coupon after weld cladding was completed. The direction of the x and y coordinate axes used in the ND strain scanning are also shown on the plan view. The z-axis is through the thickness of the plate.

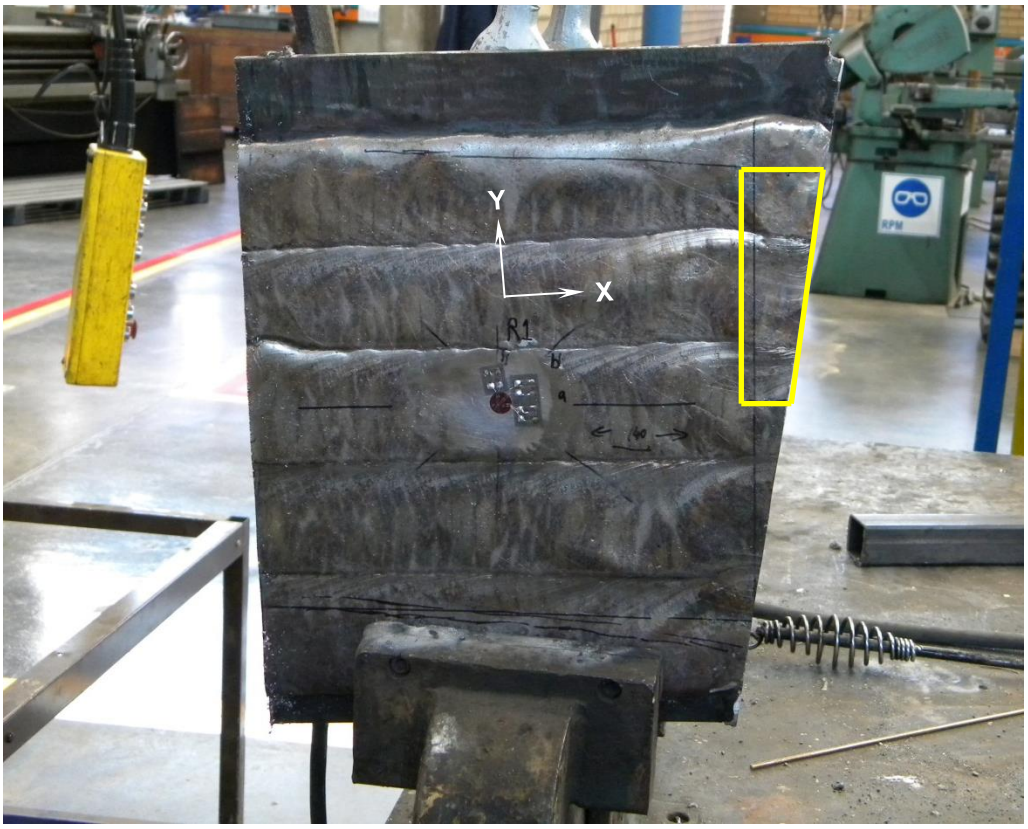

Figure 4 Clad surface of the coupon showing the quadrilateral section used to obtain stress-free reference cubes. The direction of the x and y-axes is also shown.

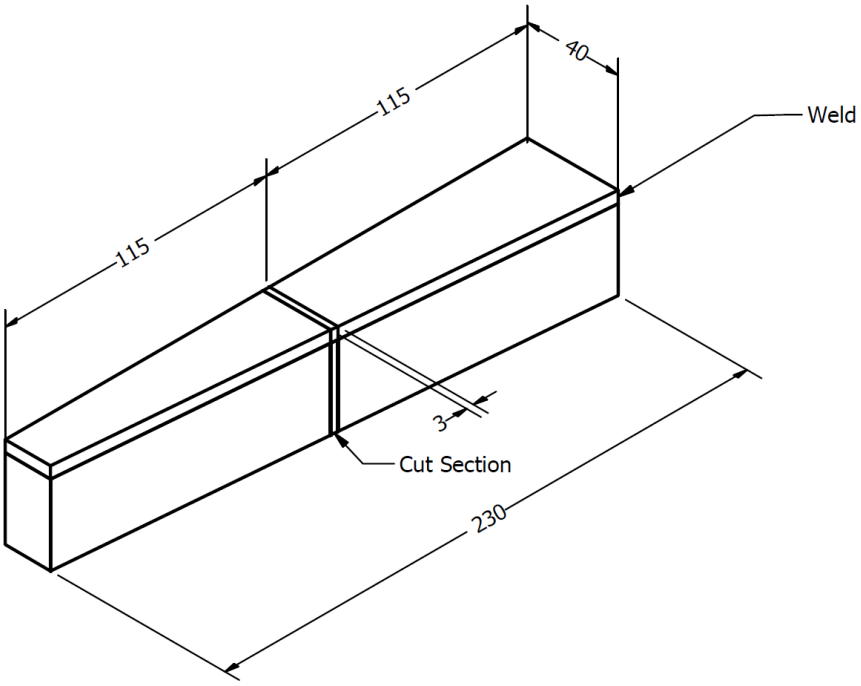

Figure 5a The central 3 mm thick slice was excised from the quadrilateral piece via EDM, polished and etched to identify the fusion boundary and then cut into the toothcomb shape shown in Figure 5b.

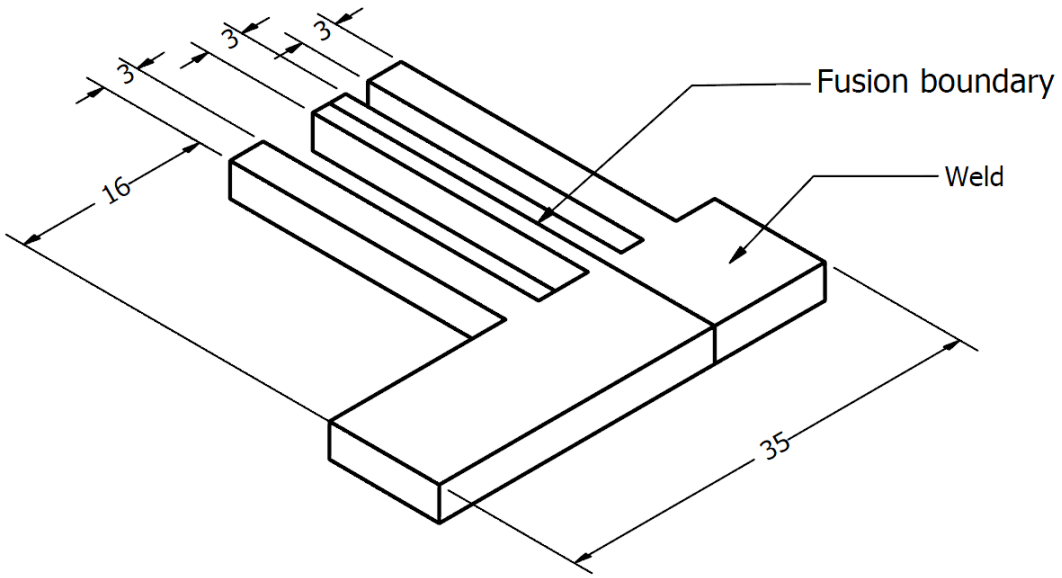

Figure 5b Schematic of the toothcomb specimen; 3 mm cubes were cut off the tooth ends to provide strain-free reference specimens.

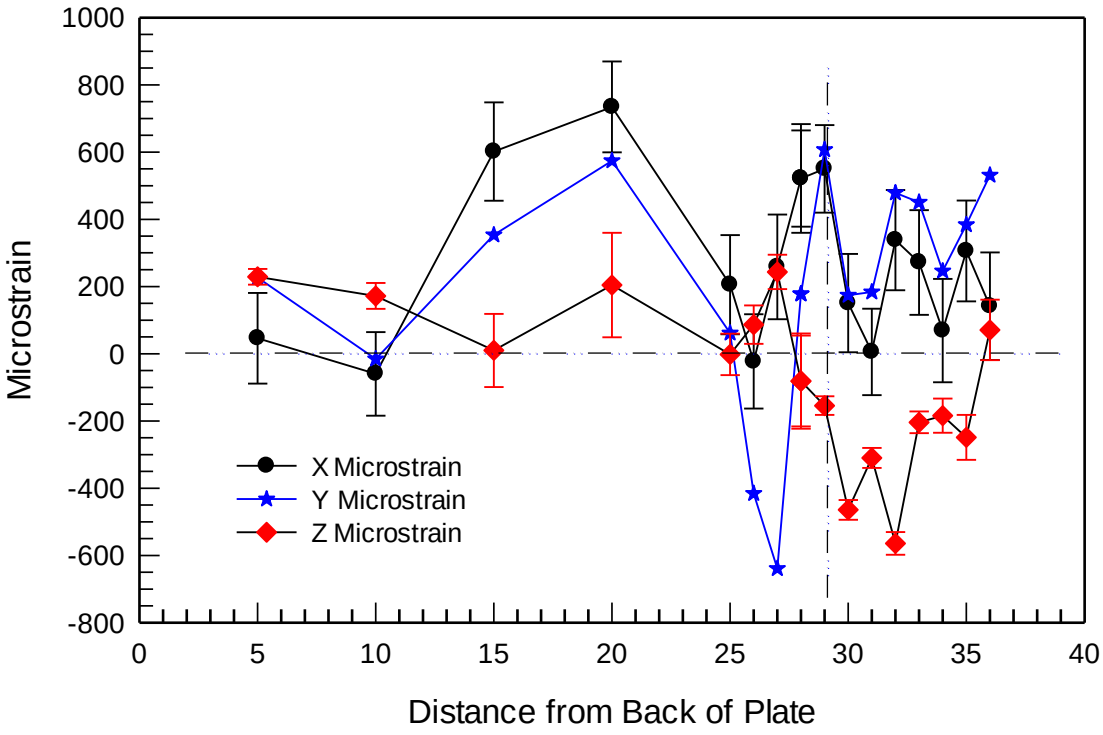

Figure 6 Residual microstrain data in all three coordinate directions as a function of *z*. Typical error bars are shown on two of the plots. The position of the weld fusion boundary is shown by the vertical line. Distances are given from the rear (unclad) surface of the plate

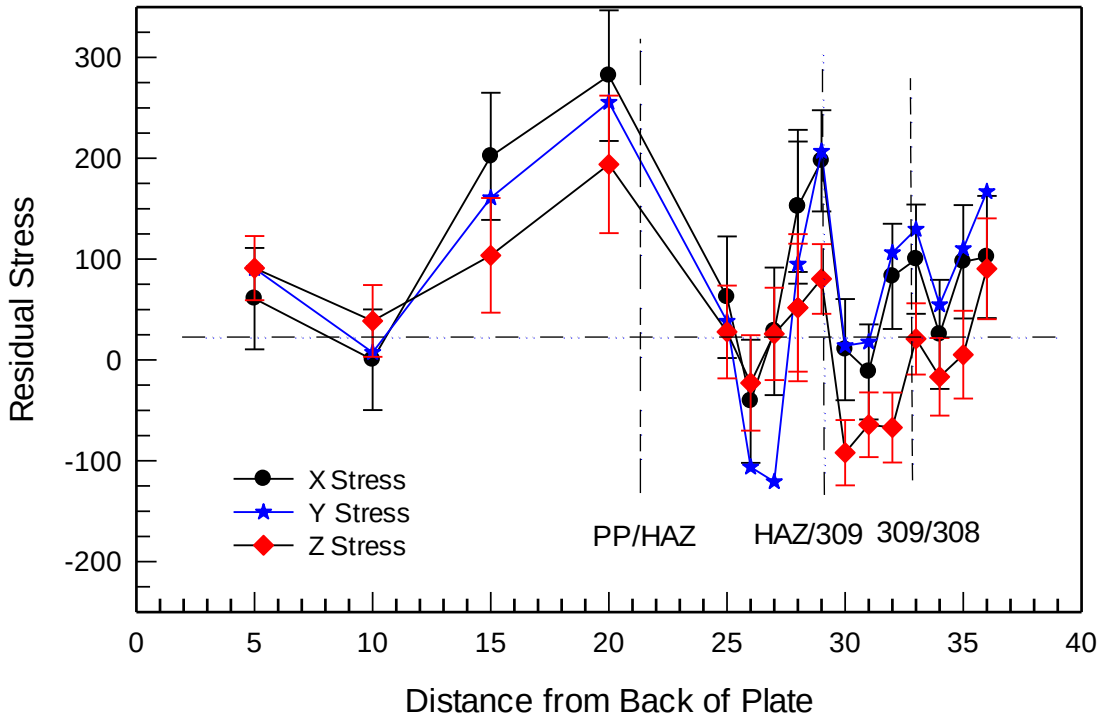

Figure 7 Residual stress data in all three coordinate directions as a function of z. Error bars are also shown. The approximate positions of the various metallurgical boundaries are shown by the vertical lines.

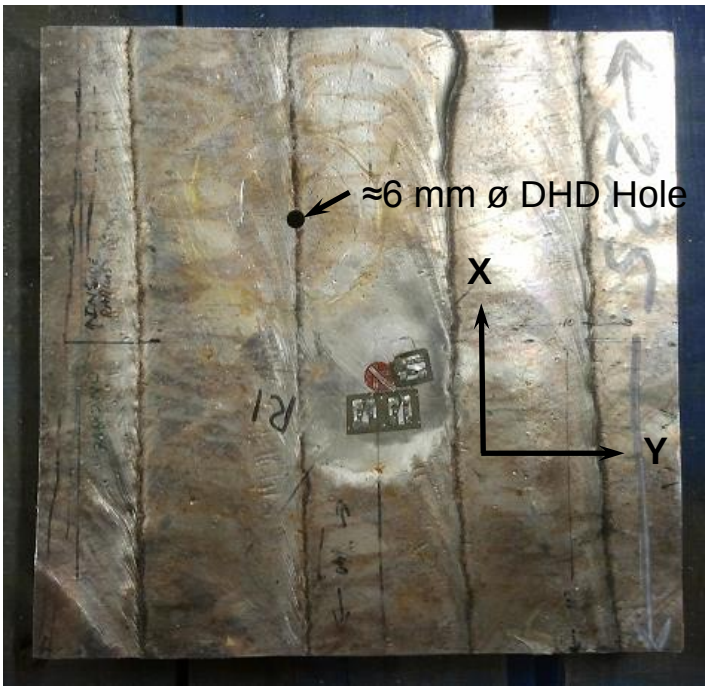

Figure 8 Position 2 on the clad plate (weld layer junction point), which was used in the residual stress measurements with both the neutron diffraction and the DHD techniques.

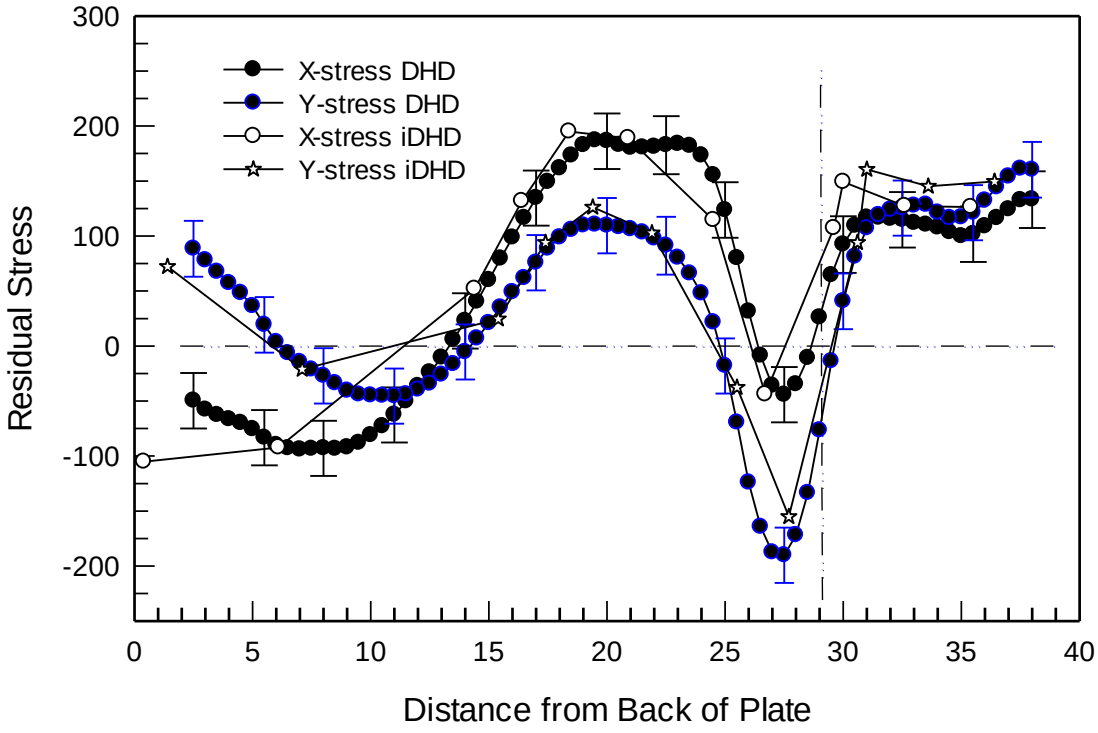

Figure 9 Longitudinal (x-direction) and transverse (y-direction) residual stress measured with DHD and incremental-DHD (iDHD) techniques. The vertical line marks the measured position of the weld fusion boundary with the parent plate (WM/PP Interface). Typical error bars are shown for the DHD data.

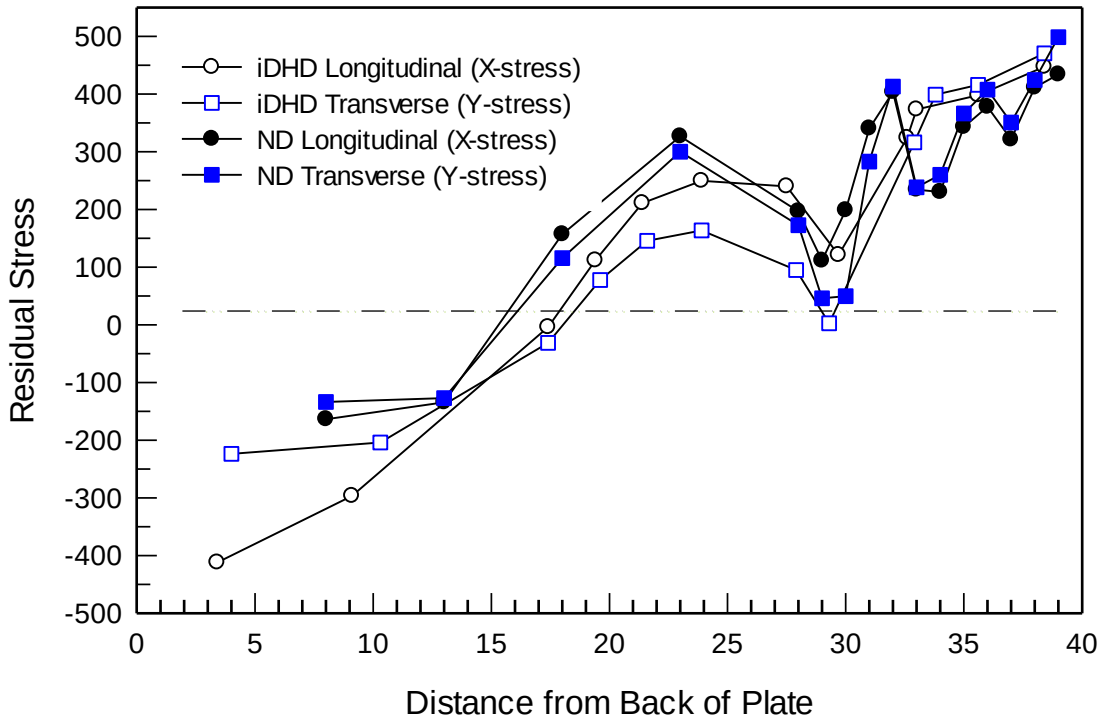

Figure 10 Comparison between the iDHD and ND residual stress after correction to account for the effect of the reduction in plate thickness from 80 mm to 30 mm.

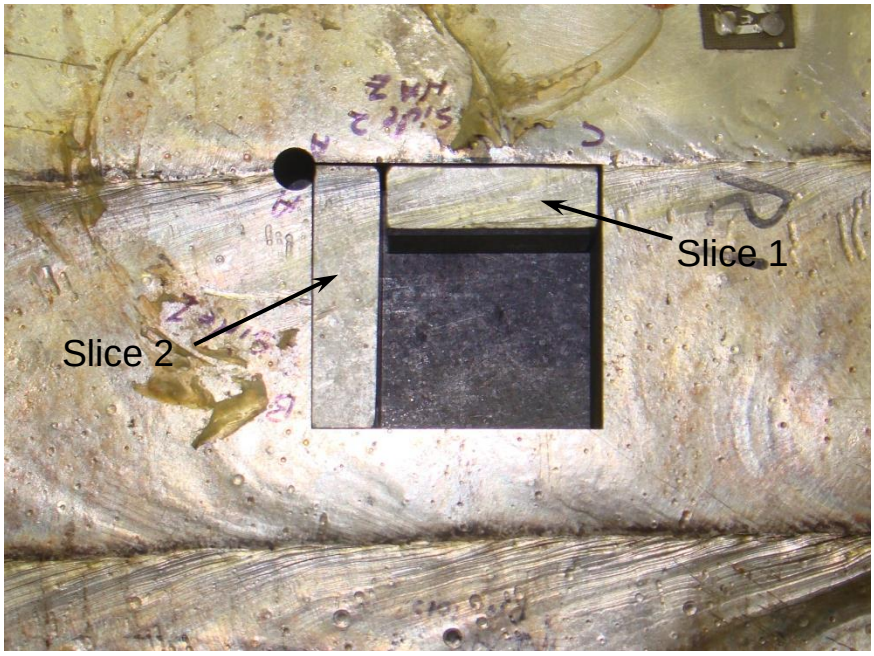

Figure 11 View of the two 10 mm thick slices that were electrodischarge machined from the welded plate to allow measurement of the thickness of the various weld zones.

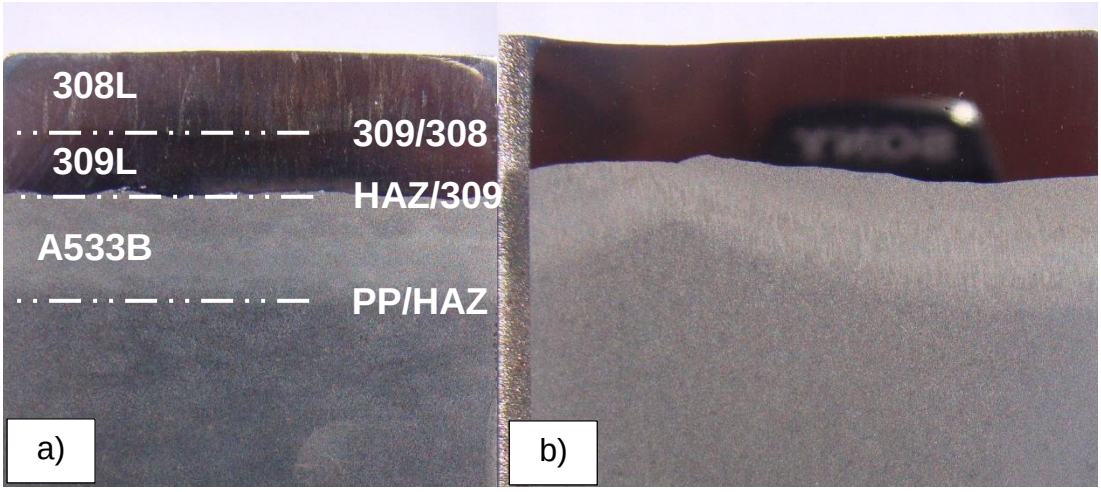

Figure 12 a) Macroetched longitudinal section of slice 1. The depth of the stainless steel cladding is fairly constant along the weld run, although a greater variation in depth of the upper layer of 308L alloy is apparent.

b) Macroetched transverse section of slice 2. The depth of the stainless steel cladding is less uniform than in the longitudinal direction.

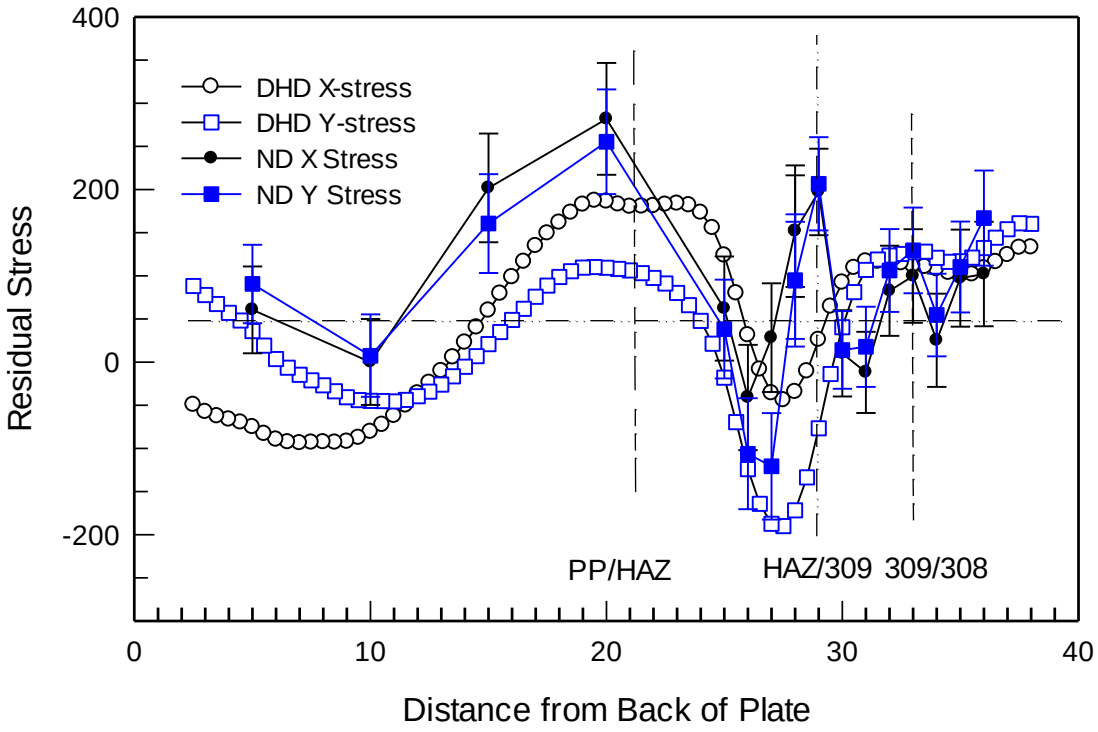

Figure 13 Comparison between the longitudinal (X-stress) and transverse (Y-stress) residual stress distributions measured with neutron diffraction (ND) and the deep-hole drilling (DHD) methods. The dashed vertical lines represent, from left to right, the measured positions of the parent plate (PP) / heat affected zone (HAZ) boundary, the weld fusion boundary (weld metal (309) / HAZ) and the fusion boundary between the 309 and 308 weld metal layers.